ADVANCED MATERIALS INTERFACES
www.advmatinterfaces.de

Revisiting the Ethylene Carbonate–Propylene Carbonate Mystery with Operando Characterization

Tim Melin, Robin Lundström, and Erik J. Berg**

The "ethylene carbonate (EC)–propylene carbonate (PC) mystery" has puzzled electrochemists for decades. Surprisingly, the minor structural difference between PC and EC, a methyl vis-à-vis a proton, prevents PC unlike EC to form a stable solid electrolyte interphase (SEI) on carbon (C), which along with the popularity of PC has impeded the development of Li-ion batteries with many years. Despite several hypotheses, the fundamental reason remains debated largely due to the lack of sufficient experimental evidence. Herein, SEI formed as a result of EC and PC reductions are analyzed by two state-of-the-art operando techniques, online electrochemical mass spectrometry and electrochemical quartz crystal microbalance with dissipation monitoring. Although both EC- and PC-based electrolytes appear to have virtually identical reaction pathways, PC is reduced much more extensively than EC and forms a much thicker SEI. However, while the SEI derived from EC remains on the electrode, PC reduction products redissolve in the electrolyte leaving the bare C electrode behind. The presented study illustrates the complex scheme of competing electro-/chemical reactions behind SEI formation and provides further scientific details needed to eventually form a consensus of the processes governing electrode/electrolyte interphases in Li-ion batteries.

1. Introduction

Electrochemical energy storage plays a critical role in the societal transition from fossil fuels to renewable energy sources. Li-ion batteries currently accelerate the electrification of the transportation sector and will eventually be key components in future electric grids. Despite the success of this battery technology, several critical components of the Li-ion cell chemistry remain unknown, which in turn impedes further development in the field. Arguably, the most critical component of any electrochemical energy storage device is the electrolyte sustaining charge transport between the two electrodes. Electrolytes for Li-ion batteries have been extensively studied, yet several crucial processes, primarily associated with their reactivity toward the electrodes, remain to be fully explained.[1] No electrolyte is intrinsically stable at the negative graphite electrode of the Li-ion battery and the reversible cell chemistry strongly relies on the formation of a solid electrolyte interphase (SEI). The SEI is a nm-thin multiphase composite layer typically formed on the graphite from degradation products of the electrolyte after the first charge/discharge cycle of the Li-ion cell. Even though a general consensus on the importance of the SEI was already established several decades ago, its formation and operating mechanisms are still intensively debated. Nevertheless, the performance of the SEI is generally observed to heavily depend on the electrolyte solvents used. The essential requirements on a solvent for a feasible Li-ion battery electrolyte are a high dielectric constant, low viscosity, broad liquid temperature interval, and sufficient stability in contact with all cell components.[1]

A group of solvents that fulfill most requirements is cyclic carbonate esters, such as ethylene carbonate (EC) and propylene carbonate (PC). The interest in EC and PC as solvents for Li batteries began in the mid-20th century after Harris showed the (electro-)chemical stability of these solvents toward alkali metals.[2] PC was most popular in the early days largely because of its wide liquid temperature range (–49 to 242 °C) compared to EC (36 to 238 °C).[1] Later, when focus shifted from Li-metal toward petroleum coke and graphite as anode for secondary lithium batteries, a clear difference between the two solvents was noticed: EC-based electrolytes outperformed PC-based electrolytes in terms of cyclability.[3] This disparity (often referred to as the "EC–PC mystery") has puzzled electrochemists ever since and has been debated extensively throughout the years.[4–10] Surprisingly, the minor difference in molecular structure between EC and PC, a proton vis-à-vis a methyl group, leads to strong differences in reactivity and degradation products of these solvents. Marked compositional differences in SEI products formed on graphite electrode depending on the choice of EC or PC was observed via ex situ ATR-FTIR analysis by Zhuang et al.[5] On the electrodes cycled in PC-based electrolyte an inorganic layer dominated by Li_2CO_3 where found, while on the electrode cycled in EC-based electrolyte a mixture of organic and inorganic species was found.

T. Melin, R. Lundström, E. J. Berg
Department of Chemistry
Ångström Laboratory
Uppsala University
Box 538, Uppsala SE-751 21, Sweden
E-mail: tim.melin@kemi.uu.se; erik.berg@kemi.uu.se

The ORCID identification number(s) for the author(s) of this article can be found under https://doi.org/10.1002/admi.202101258.

DOI: 10.1002/admi.202101258

Therefore, solvent-dependent differences in reaction pathways were suggested. Alternative to a hypothesis of molecular structure-dependent reactivity, an explanation based on the solvent's ability to co-intercalate with Li^+ into graphite has been presented.[11] PC co-intercalation leads to an increased distance between the graphene layers, resulting in unwanted volume expansion and severe mechanical strain with particle cracking, graphite exfoliation, and rapid capacity loss, while little to no co-intercalation is present in EC-based electrolytes.[12,13] Such severe side-reactions could in model SEI studies be effectively ruled out by employing an electrode material mimicking the prismatic surface of graphite but not permitting for solvent co-intercalation with Li^+, such as glassy carbon (GC) for which Li^+ adsorption is the dominating charge-storage mechanism. A third hypothesis has been presented in a study by Xu[8] where he suggests that the same reaction pathways for both solvents, but that the poorer performance of PC rather stems from the inability of its reduction products to stick to the negative electrode surface because of their higher solubility in the electrolyte. Both EC and PC form dicarbonates, namely lithium ethylene dicarbonate (LEDC) and lithium propylene dicarbonate (LPDC), upon reduction,[14,15] but only LEDC proposedly form an effective SEI stabilizing the negative Li-ion electrode during further cycling.

In spite of more than thousands of published studies, the SEI is generally considered elusive because of its dynamic nature with a structure evolving over time and including several metastable phases. The lack of suitable in situ or operando analytical techniques, capable of characterizing the SEI during formation and operation, is a major impediment in the field. One technique gaining more attention is online electrochemical mass spectrometry (OEMS), which combines a battery with a mass spectrometer to monitor the evolution of volatile species during operation of the cell. Recently, our team developed an OEMS setup capable of determining not only the evolution rates of the most commonly observed gases during SEI formation, such as H_2, CO_2, and C_2H_4, but also establishing their individual contribution to the total gassing of the cell.[16] Another suitable analytical technique widely employed to study electrochemical systems in situ and operando is electrochemical quartz crystal microbalance (EQCM), which may monitor mass deposition on model electrodes during operation with unparalleled sensitivity. For instance, Aurbach and Zaban[6] studied SEI formation on model Au electrodes in contact with PC-based electrolyte and compared how the salt composition ($LiPF_6$ and $LiAsF_6$) of electrolyte affect the SEI. More importantly, they additionally demonstrated that the SEI composition does not solely depend on the choice of base electrolyte components, but also on the presence of electrolyte impurities. In 2020, Kitz et al.[17] published a similar study where SEI formation on model carbon (C) electrodes in contact with EC-based electrolyte was studied with EQCM complemented by OEMS. Here, a clear difference between dry and water contaminated electrolytes was also confirmed. The onset potential at which the SEI starts forming for the contaminated electrolyte was 2.4 V versus Li^+/Li where a rigid and thick inorganic layer starts growing, while the onset potential for SEI formation in a nominally dry electrolyte was significantly lower (1.7 V vs Li^+/Li) and a much thinner layer was observed. Due to development of the EQCM including dissipation monitoring (EQCM-D), viscoelastic properties of these layers could also be obtained. It was found that the layer in the water contaminated electrolyte was not only thicker, but also more rigid. The onset potential where the rigid layer starts growing correlated well with CO_2 evolution in the OEMS measurements, which confirms the hypothesis that hydroxide ions from water reduction, catalyzes a ring-opening of EC forming alkoxides and CO_2. Hydroxide ions react further with CO_2 forming lithium carbonate which results in a rigid SEI.

Trace amounts of contaminants, such as H_2O, alter the SEI composition regardless of the salt and/or solvent used and is well-known to degrade the performance of the SEI and in turn the whole battery cell. Comparing SEIs formed in electrolytes containing varying levels of impurities, even on the ppm-level, will not give the same results. This holds especially true for battery lab cells with high flooding factors, such as the ones available for OEMS and EQCM today. The flooding factor is defined as the ratio of electrolyte volume to electrode area, and means in effect that larger volumes of electrolyte carries a larger number of contaminants available to react per electrode surface area. The influence of electrolyte impurities therefore grows with increasing flooding factors, and we believe this is a major challenge partly explaining the vast number of disparate results on SEI in existing literature. Impurities are notoriously difficult to eliminate and must instead be systematically accounted for when studying the SEI. Revisiting well-studied systems, such as the SEI, but with strict control of impurities, is therefore warranted.

Herein, OEMS and EQCM-D are combined to study the SEI formation in a common EC-based electrolyte (1 M $LiPF_6$ in EC:DEC [1:1 vol%], referred to as EC or EC electrolyte) and a PC-based electrolyte (1 M $LiPF_6$ in PC, referred to as PC or PC electrolyte) during the first lithiation step of C. GC is employed as model electrode substrate to effectively disregard effects associated with PC/EC co-intercalation with Li^+. The study aims to provide deeper insights into and further support for the hypothesis that the choice of PC as opposed to EC as base solvent leads to a larger amount of degradation products incapable of stabilizing the SEI on C because of their higher solubility.

2. Results and Discussion

2.1. Gas Evolution Analysis during First Lithiation of Carbon in Ethylene Carbonate- and Propylene Carbonate-Based Electrolytes

Figure 1 presents the electrochemical potential profile during constant current (–1 μA cm^{-2}) lithiation of porous GC electrodes in EC electrolyte (filled squares) and PC electrolyte (open squares) along with their respective gas evolution rates. H_2, CO_2, and the alkenes are the dominating volatile compounds formed. The lithiation potentials of GC in the two electrolytes are similar and governed by Li^+ adsorption in the surface structures of these carbons.[6] The potential of the PC-based cell deviates however slightly from the expected profile

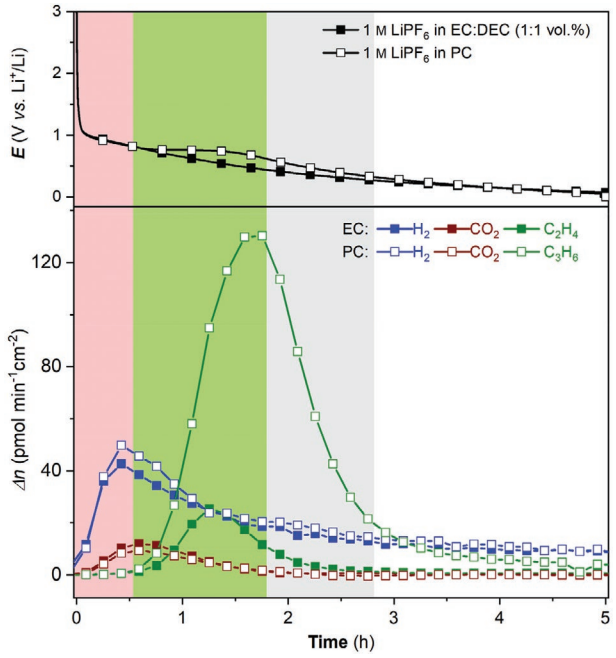

Figure 1. Potential profiles, E, and associated gas evolution rates Δn of H_2 (in blue), CO_2 (in red), and C_2H_4/C_3H_6 (in green) from OEMS measurements of porous glassy carbon electrodes in 1 M LiPF6 in EC:DEC (1:1 vol%) (solid squares) and 1 M $LiPF_6$ in PC (open squares).

with a plateau at 0.9 V (after ≈1 h, marked interval in green, Figure 1), which correlates well with the anticipated potential for PC (and EC) reduction and the evolution of propylene (and ethylene):

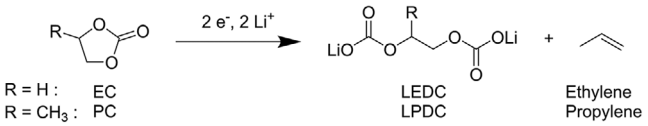

(1)

This single-electron (per EC/PC molecule) reduction pathway of cyclic carbonates (Equation (1)), in which one alkene and one dicarbonate (LEDC for EC and LPDC for PC) are formed per reaction, are well-established in the literature concerned with SEI formation in non-aqueous organic carbonate-based electrolytes.[1,18] LEDC (or derivatives thereof) is a generally presumed and essential constituent of the SEI passivation layer on the carbons. The absence of a clear potential plateau for reduction of EC is simply due to the more efficient SEI passivation in the EC electrolyte, which significantly lowers its influence on the electrode potential. In other words, the reduction process of PC is different to EC, the electrode is not as efficiently passivated by the reduced PC species, which leads to more PC reduction and the establishment of a potential plateau at 0.8 V. Comparing the alkene evolutions, it is clear that the amount of ethylene evolved in the EC cell is much lower than propylene evolved in the PC cell, which correlates well with the reasoning above. By integrating the alkene evolution, an estimation of the total number of dicarbonates formed is possible: ≈1.4 nmol cm^{-2} ethylene is formed on the GC electrode in EC and ≈10.1 nmol cm^{-2} propylene in the PC electrolyte. These amounts of alkenes would according to Equation (1) correspond to layers of LEDC and LPDC of 1.76 and 14 nm respective thicknesses, assuming a density of 1.3 g cm^{-3} for both dicarbonates and a uniform coverage.

For both electrolytes, H_2 evolution starts almost instantaneously as the current starts flowing and the potential drops (red interval, Figure 1). The two primarily expected electrochemical processes contributing to H_2 evolution are reduction of HF and H_2O cell impurities (Equations (2) and (3)), which are triggered by electrode potential <2.5 and <1.8 V, respectively:

$$HF + e^- + Li^+ \rightarrow LiF + 1/2H_2 \quad (2)$$

$$H_2O + e^- \rightarrow OH^- + 1/2H_2 \quad (3)$$

The integrated H_2 evolution would correspond to 2.74 and 3.04 µmol reduced protons in the cell with EC and PC electrolyte, respectively. The concentration of HF was experimentally determined to be ≈100 ppm in both electrolytes prior to cell assembly. If all HF is assumed to be reduced and the remaining H_2 originate from H_2O, the cell impurity concentration of H_2O would be 70 and 90 ppm for EC and PC electrolyte, respectively. These H_2O concentrations are higher than measured via Karl-Fischer titration performed before assembly (≈20 ppm), but the additional H_2O content in the cells is expected and likely originates from the electrodes and other cell parts in contact with the electrolyte. Although both electrodes and other cell parts were vacuum-dried at elevated temperatures (see Experimental Section), H_2O is notoriously difficult to remove completely. The CO_2 evolution profiles in both electrolytes are virtually identical, which supports the same scenario. Reduction of H_2O leads to OH^- formation, which is known to catalyze the ring-opening of PC/EC[19] (Equations (4) and (5)).

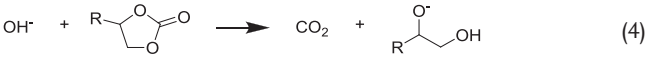

(4)

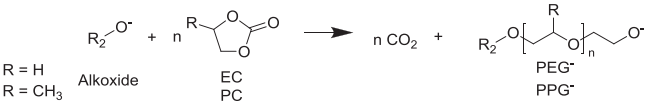

(5)

Indeed, CO_2 forms after H_2 and evolves to the same extent regardless of the cyclic carbonate, thus evidencing its origin from secondary reactions independent of EC/PC reduction (no CO_2 evolution is detected after the alkene evolution). The influence of H_2O contamination on SEI formation on C electrodes has been investigated in several studies[17,18] and the resulting SEI products vary strongly depending on the electrolyte purity. A dry electrolyte produces more ethylene while a wet produces more CO_2. The amounts of CO_2 and ethylene evolved in the EC-based electrolyte are in line with previous observations.[17]

2.2. Mass Deposition on Carbon during Its First Lithiation in Ethylene Carbonate- and Propylene Carbonate-Based Electrolytes

Figure 2 presents the potential profile of the C-coated QCM sensor in contact with 1 M LiPF6 in EC:DEC (1:1 vol%) during the first constant current (–5 µA cm^{-2}) lithiation step along with the associated deposited mass, its viscoelastic properties, and the viscosity of the nearby electrolyte. The potential profile displays again a continuously decreasing slope, similar to GC in the OEMS experiment (Figure 1) and reminiscent of Li^+ adsorption being the electrochemically governing process. Four distinct intervals may be identified (color coded in red, green, gray, and white in Figure 2) according to the applied electrochemical protocol and the viscoelastic response of the sensor. Straight after cell assembly (white interval, Figure 2), the cell rests at open circuit voltage (OCV) of ≈3 V with no appreciable mass formation on the sensor. When the negative current is applied, the electrode potential monotonically drops and mass deposition onsets immediately (red interval). A minor potential plateau ≈2 V is however discerned and correlates to the H_2 evolution observed in OEMS (Figure 1). Unfortunately, since there is insufficient deposition and/or interphasial change in this interval the viscoelastic Voigt-model falls short and no real fit solution is found until 0.4 h (vertical dashed line, Figure 2) into the experiment. However, by recognizing the cumulated deposited mass of 0.9 µg cm^{-2} at the same point and the charge consumed after starting the experiment (4 mAs) an overall mass-per-electron (mpe) value of 25 g mol^{-1} e$^-$ is calculated, which agrees roughly with what is expected for the deposition of LiF (mpe = 27 g mol^{-1}). About 1/6 of all HF expected to be present in the cell would be consumed at this point. If a uniform layer of LiF on the C-sensor would be formed, its thickness would be ≈3 nm, which should be sufficient to passivate the C-sensor. According to DFT calculations performed by Lin et al., already a 2 nm LiF layer would block electron tunneling and passivate the electrode.[20] This implies in turn that LiF does not grow as homogenously dense films on the electrode, but rather form larger aggregates as previously observed by AFM measurements on C.[21] Such mass deposits differ in thickness with one order of magnitude from that estimated from the H_2 evolution reaction and the porous electrodes in OEMS cell (≈0.6 nm). An explanation can however be found in the difference in flooding factors of the two electrochemical cells. In the EQCM, roughly 400 µL electrolyte is used for 1.13 cm^2 electrode, while in the OEMS cell, 300 µL electrolyte is used with a 260 cm^2 electrode. In the EQCM-D cell there is simply much more HF present per surface area of electrode and thicker layers of reduction products are expected. The larger amount of HF reduced per electrode surface area equally well explains the appearance of the potential plateau. The viscosity of the electrolyte phase is constant around 3.3 mPa s, which is lower than the viscosity of the EC electrolyte found in literature (≈4 mPa s)[22] and might be due to H_2 gas bubble formation on the sensor. The SEI viscosity is significantly higher (≈20 mPa s) and likely represents a mixed effective value for the already slightly porous deposit. When we approach 1 V, the mass increases already at a lower rate with an mpe of ≈15 g mol^{-1}. One reason for this low mpe-value could be that portions of the charge are now consumed by reduction of H_2O, which has no solid product. A second reason is that Li^+ adsorption (mpe = 7 g mol^{-1}) on the C-surface already kicked in. Despite this mixed scheme of competing electrochemical processes, the observation of a stable mpe in the latter part of the red interval indicates that the fractions of participating reactions are rather constant.

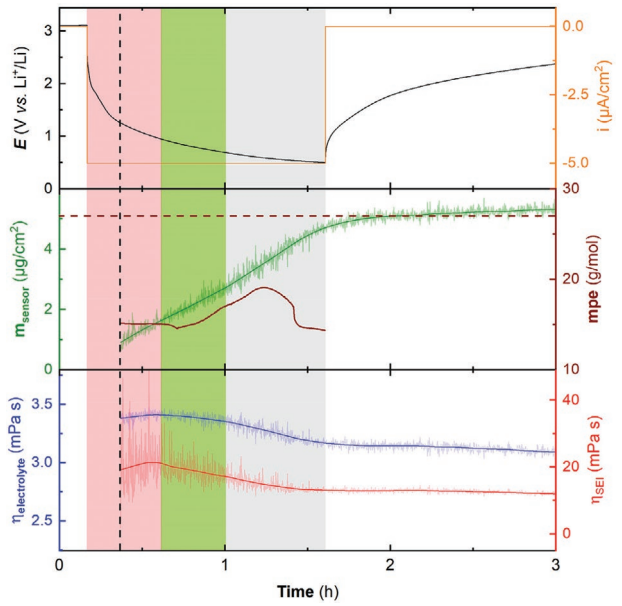

Figure 2. Electrode potential, *E*, of a carbon-coated QCM sensor during the first galvanostatic (–5 µA cm^{-2}) lithiation step to down to 0.5 V in 1 M LiPF6 in EC:DEC (1:1 vol%) electrolyte along with the mass and viscoelastic properties of the deposited layers and the viscosity of the nearby electrolyte.

Below 1 V (green interval, Figure 2) the mass deposition rate first slightly decreases and then again increases as observed from the mpe values. OEMS evidenced the reduction of EC at the same potentials and the formation of gas (i.e., C_2H_4), which first would lower the mpe values (no mass deposit) and later significantly increase the mpe values when the products of EC reduction reach their solubility limits (e.g., LEDC is 81 g mol^{-1}, Li_2CO_3 is 37 g mol^{-1}). Even though the mpe values in 0.9 V < *E* < 0.6 V remain relatively low (mpe^{max} ≈ 20 g mol^{-1}), they likely evidence EC reduction, but result from a mixed reaction scheme dominated by Li^+ adsorption, judging from the sloping potential profile. At *E* < 0.6 V, the mpe-value decreases to ≈15 g mol^{-1} before the current is interrupted, which now indicates a largely passivated C-sensor and an electrode potential largely dominated by Li^+ adsorption. The decreasing electrolyte and SEI viscosities may at the same time (green and gray interval) reflect a larger fraction of organic and possibly solvated compounds in the SEI. In the white region (OCV after constant current step), the electrode mass stabilizes with no apparent dissolution of the SEI observed.

Figure 3 presents the potential profile of the C-coated QCM sensor in contact with 1 M $LiPF_6$ in PC as electrolyte during the first constant current (–5 µA cm^{-2}) lithiation step together with the associated deposited mass, its viscoelastic properties, and the electrolyte viscosity. Based on the electrode potential,

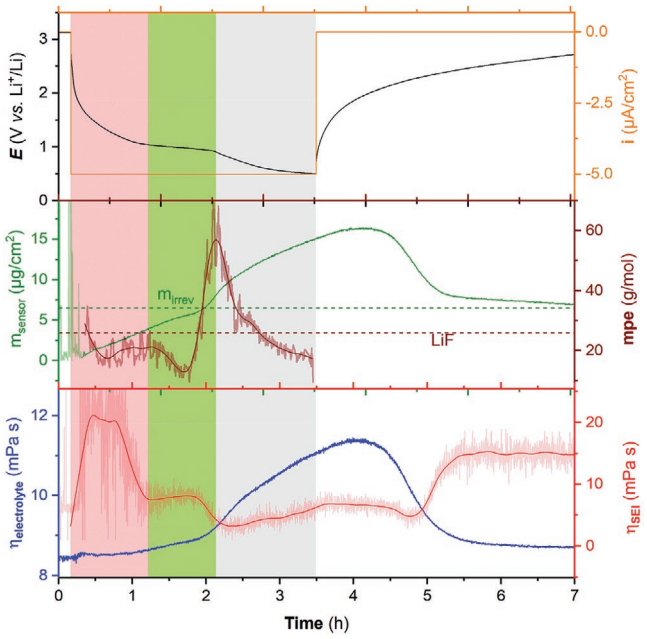

Figure 3. Electrode potential, *E*, of a carbon-coated QCM sensor during the first galvanostatic (−5 μA cm^{-2}) lithiation step to down to 0.5 V in 1 M $LiPF_6$ in PC along with the mass and viscoelastic properties of the deposited layers and the viscosity of the nearby electrolyte.

four intervals are identified of which the three first intervals (marked in red, green, and gray) display several similar characteristics to the EC cell, while the last interval demonstrates a clearly deviating mass dissolution phase (white).

From OCV to 1 V (red interval, Figure 3), HF and H_2O reduction are expected to occur. Despite the similar impurity concentrations of the EC- and PC-based electrolytes (≈100 ppm HF, ≈30–40 ppm H_2O), the latter render ≈2× larger consumed charge and ≈2× C-sensor mass deposits >1 V. In addition, the mpe values for PC are also higher (≈20 g mol^{-1} in average) compared to EC, hence evidencing a stronger dominance of mass deposition as opposed to Li^+ adsorption on the C. Among the various factors that may explain this observation, HF/H_2O mass transport and product solubilities are expected to be different in EC- and PC-based electrolytes and significantly influence the SEI formation. A higher solubility of a reduction product would promote growth of larger aggregates, such as the micron-sized LiF crystallites previously observed as part of the SEI on C, which would passivate the C-sensor to a lesser extent and allow electrolyte reduction to proceed for a longer time. The initially recorded SEI viscosity is ≈20 mPa s, which is the same as for EC electrolyte and implies similar early mass deposits in both electrolytes. The electrolyte viscosity increased only marginally (≈0.3 mPa s) from its starting value, which in turn agrees very well with previous ex situ measurements (8.4 mPa s).[23]

Both the SEI viscosity and the mpe value drop at 1 V (green interval, Figure 3) in a similar fashion, but to a much greater extent compared to EC electrolyte (green interval, Figure 2). PC reduction and the formation of gaseous (C_3H_6) and soluble products (LPDC) at the C-sensor are indeed expected to be more substantial compared to EC judging from the OEMS results (Figure 1). Once the concentration of LPDC close to the sensor exceeds its solubility, precipitation starts, mass deposition accelerates, and the SEI viscosity decreases. Although the observed peak mpe value (≈60 g mol^{-1}) is close to the expected value for LPDC (88 g mol^{-1}), PC reduction is eventually overtaken by Li^+ adsorption as both the mpe value and potential are observed to drop. Interestingly, the mass on the C-sensor keeps increasing in a coordinated fashion with the electrolyte viscosity (gray interval, Figure 3), even after current cut-off. Such a process—independent of electrode potential (increases rapidly after cut-off) and charge flow—must be purely chemical in nature and likely governed by reactions in the electrolyte solution close to the C-sensor. Reduced PC radicals formed <1 V may for instance have a sufficiently long lifetime to diffuse and alter the physicochemical properties of the electrolyte, before reacting and precipitating as LPDC (Equation (1)). Mass deposition associated with this process (10 μg cm^{-2}) would correspond to almost 80 nm LPDC, which is far more than necessary to passivate the electrode. These products of PC reduction are however soluble and eventually diffuse away from the C-sensor, since its mass again decreases and the electrolyte and SEI viscosities return to their respective values (8.5 and 20 mPa s) compared to before the PC reduction set in. Only the insoluble products, such as LiF and/or Li_2CO_3, remain on the C-sensor.

3. Summary and Conclusions

Herein, we present a detailed comparison of the SEI formation processes on C in EC- and PC-based electrolytes by combining operando gas (OEMS) and mass deposition (EQCM-D) analysis. Operando analysis is demonstrated to both qualitatively and quantitatively capture several steps of the reaction dynamics spanning from electrolyte impurity and solvent reduction to product formation, speciation, and saturation in the electrolyte along with precipitation on the electrode. Our results demonstrate that complementary analytical techniques are necessary to gain a complete picture of the reaction processes considering their complexity as well as the multitude of volatile, soluble, and solid reactants involved. Based on the experimental observations above, a detailed reaction scheme may be presented (**Figure 4**).

Regardless of the electrolyte, HF and H_2O impurities are reduced early ($E > 1$ V) forming H_2 (g) along with a rigid solid layer on the electrode (red interval in Figure 4), likely predominantly consisting of LiF and Li_2CO_3 as confirmed spectroscopically in previous studies.[24] Although sufficient deposits to completely passify the electrode are formed, the precipitation process of these inorganic compounds is likely governed by nucleation and growth of larger aggregates, which only marginally limits the access of the electrolyte to the electrode surface. Evidence of incomplete electrode passivation is observed at lower potentials ($E < 1$ V, green interval in Figure 4) when both EC and PC are reduced. The formation of volatile alkenes (C_2H_4 and C_3H_6) is not only observed by OEMS, but also by EQCM-D in form of lower mpe values and SEI viscosities. Heavier products of carbonate solvent reduction rapidly overtake the electrode mass build-up process, as represented by

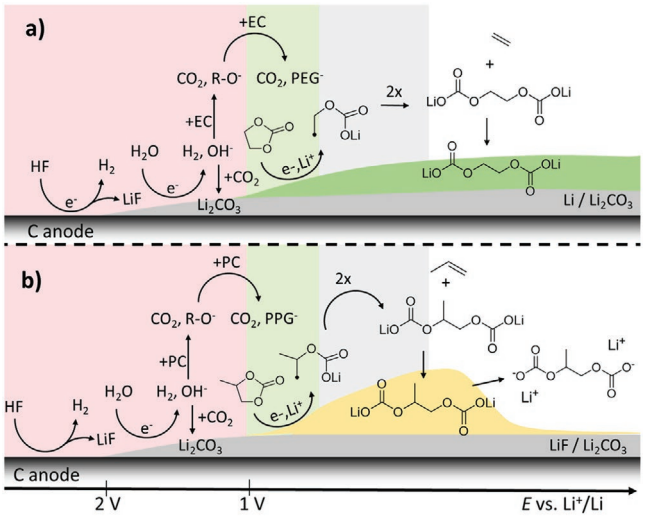

Figure 4. Schematic of the SEI formation process in a) EC-based electrolyte and b) PC-based electrolyte.

LEDC and LPDC in Figure 4, until the electrode is sufficiently passivated to allow for complete lithiation of the C. The most obvious difference between the EC- and PC-based electrolytes is their respective ability to form a stable SEI. Even though PC reduction is much more extensive than EC reduction (larger amount of C_3H_6 compared to C_2H_4 is evolved) and a significantly thicker interphase is formed, the SEI layer formed in PC eventually completely dissolves leaving only the initially formed inorganic mass deposits on the electrode. These findings confirm Xu's hypothesis[8] that PC reduction products are ineffective SEI formers due to their significantly higher electrolyte solubilities compared to EC derived products. Simulations performed by Takenaka et al. indicated, for instance, that the additional methyl group in PC (as opposed to the proton on EC) would result in much poorer packing density of precipitated LPDC compared the LEDC counterpart.[10] Since graphite exfoliation is not the cause, but rather the effect of a poorly passivating SEI, successful strategies for reversible cycling of graphite must hence guarantee the formation of an efficient SEI, for example, by including layer-forming additives,[25–27] preformed electrode coatings,[28,29] or high electrolyte salt concentrations.[30,31] Although more details underpinning the poor SEI forming capability of PC remain to be discovered, our operando study provides undisputable evidence of product dissolution as a serious SEI failure mechanism. We experimentally demonstrate that SEI formation is based on a complex scheme of competing electrochemical and chemical reactions, which continue to proceed even after the galvanostatic current is cut. Even if the EC versus PC mystery will continue to be debated, the methodology and scientific details presented herein provide further building-blocks needed to eventually establish a consensus on the governing reaction mechanisms behind SEI formation.

4. Experimental Section

Porous GC electrodes were prepared by mixing 95 wt% GC powder (Sigma-Aldrich, spherical powder, 2–12 µm, 99.95% trace metals basis, Sweden) and 5 wt% PVDf (Kynar Flex 900 HSV, Arkema, France) binder in *N*-methyl-2-pyrrolidone (Sigma-Aldrich, Sweden) solution. The solution was mixed for 30 min at 25 Hz (MM 400, Retsch, Germany). The slurry was coated on a stainless-steel mesh (212/90 µm, Bopp AG, Switzerland) with a 150 µm gap applicator. Carbon QCM-sensors were prepared by coating commercial 5 MHz Au type sensors (Q-Sense, Biolin Scientific AB, Sweden) with first a 50 nm thick Cr adhesion film and then a 50 nm thick C layer by sputter deposition at room temperature. $LiFePO_4$ electrodes (Custom cells, 2 mAh cm^{-2}, Germany) were punched (ϕ 15 mm for the OEMS cell, ϕ 12 mm for the EQCM cell) and delithiated to 3.43 V versus Li^+/Li. All electrodes used where dried at 120 °C for 12 h in a vacuum oven before cell assembly.

1 M $LiPF_6$ in EC:DEC (1:1 vol%, 99.9%) and 1 M $LiPF_6$ in PC (99.9%) were bought from Solvionic (France) and used as received. Before cell assembly, H_2O and F^- concentrations were experimentally determined for both electrolytes via Karl–Fischer titration and free F^- ion sensitivity probe.[21] Approximately 20 ppm H_2O and approximately 100 ppm HF were found in both electrolytes.

The electrochemical cells and the data treatment procedure for operando measurements are described in previous publications.[16,17,32] All electrode potentials were presented relative to the Li^+/Li redox couple. $LiFePO_4$ counter electrode was assumed to be stable at 3.43 V, since negligible polarization was expected due to the low currents used.

The C electrodes were cycled against $LiFePO_4$ with a constant current (–1 µA cm^{-2} for OEMS and –5 µA cm^{-2} for EQCM-D) from OCV to a cut-off potential (0.05 V vs Li^+/Li for OEMS and 0.5 V vs Li^+/Li for EQCM). The higher cut-off potential for the EQCM measurements was applied to avoid the risk of lithiation of the Au layer beneath the Cr/C layer. This should be possible since the Cr/C layer was covering the whole surface which was in contact with the electrolyte, but cracks and pinholes might be present in the sputtered layer.

Acknowledgements

The authors acknowledge Knut and Alice Wallenberg (KAW) Foundation (Grant 2017.0204) and Swedish Research Council (2016-04069) for financial support. StandUp for Energy is acknowledged for base funding.

Conflict of Interest

The authors declare no conflict of interest.

Data Availability Statement

Data available on request from the authors.

Keywords

electrochemical quartz crystal microbalance with dissipation monitoring, Li-ion batteries, online electrochemical mass spectrometry, operando, solid electrolyte interphases

Received: July 16, 2021
Revised: September 1, 2021
Published online: October 31, 2021

[1] K. Xu, *Chem. Rev.* **2014**, *114*, 11503.
[2] W. S. Harris, *Electrochemical Studies in Cyclic Esters*, Ph.D. Thesis, University of California, Berkeley, CA **1958**.
[3] R. Fong, U. von Sacken, J. R. Dahn, *J. Electrochem. Soc.* **1990**, *137*, 2009.

[4] X. Zhang, R. Kostecki, T. J. Richardson, J. K. Pugh, P. N. Ross, *J. Electrochem. Soc.* **2001**, *148*, A1341.
[5] G. V. Zhuang, H. Yang, B. Blizanac, P. N. Ross, *Electrochem. Solid-State Lett.* **2005**, *8*, A441.
[6] D. Aurbach, A. Zaban, *J. Electroanal. Chem.* **1995**, *393*, 43.
[7] L. Xing, X. Zheng, M. Schroeder, J. Alvarado, A. Von Wald Cresce, K. Xu, Q. Li, W. Li, *Acc. Chem. Res.* **2018**, *51*, 282.
[8] K. Xu, *J. Electrochem. Soc.* **2009**, *156*, A751.
[9] M. E. Spahr, T. Palladino, H. Wilhelm, A. Würsig, D. Goers, H. Buqa, M. Holzapfel, P. Novák, *J. Electrochem. Soc.* **2004**, *151*, A1383.
[10] N. Takenaka, Y. Suzuki, H. Sakai, M. Nagaoka, *J. Phys. Chem. C* **2014**, *118*, 10874.
[11] H.-L. Zhang, C.-H. Sun, F. Li, C. Liu, J. Tan, H.-M. Cheng, *J. Phys. Chem. C* **2007**, *111*, 4740.
[12] L. J. Hardwick, H. Buqa, M. Holzapfel, W. Scheifele, F. Krumeich, P. Novák, *Electrochim. Acta* **2007**, *52*, 4884.
[13] J. O. Besenhard, M. Winter, J. Yang, W. Biberacher, *J. Power Sources* **1995**, *54*, 228.
[14] D. M. Seo, D. Chalasani, B. S. Parimalam, R. Kadam, M. Nie, B. L. Lucht, *ECS Electrochem. Lett.* **2014**, *3*, A91.
[15] G. V. Zhuang, K. Xu, H. Yang, T. R. Jow, P. N. Ross, *J. Phys. Chem. B* **2005**, *109*, 17567.
[16] R. Lundström, E. J. Berg, *J. Power Sources* **2021**, *485*, 229347.
[17] P. G. Kitz, P. Novák, E. J. Berg, *ACS Appl. Mater. Interfaces* **2020**, *12*, 15934.
[18] S. J. An, J. Li, C. Daniel, D. Mohanty, S. Nagpure, D. L. Wood, *Carbon* **2016**, *105*, 52.
[19] M. Metzger, B. Strehle, S. Solchenbach, H. A. Gasteiger, *J. Electrochem. Soc.* **2016**, *163*, A1219.
[20] Y. X. Lin, Z. Liu, K. Leung, L. Q. Chen, P. Lu, Y. Qi, *J. Power Sources* **2016**, *309*, 221.
[21] D. Strmcnik, I. E. Castelli, J. G. Connell, D. Haering, M. Zorko, P. Martins, P. P. Lopes, B. Genorio, T. Østergaard, H. A. Gasteiger, F. Maglia, B. K. Antonopoulos, V. R. Stamenkovic, J. Rossmeisl, N. M. Markovic, *Nat. Catal.* **2018**, *1*, 255.
[22] S. I. Lee, U. H. Jung, Y. S. Kim, M. H. Kim, D. J. Ahn, H. S. Chun, *Korean J. Chem. Eng.* **2002**, *19*, 638.
[23] T. Nishida, K. Nishikawa, Y. Fukunaka, *ECS Trans.* **2019**, *6*, 1.
[24] N. Mozhzhukhina, E. Flores, R. Lundström, V. Nyström, P. G. Kitz, K. Edström, E. J. Berg, *J. Phys. Chem. Lett.* **2020**, *11*, 4119.
[25] Y. Hu, W. Kong, Z. Wang, H. Li, X. Huang, L. Chen, *Electrochem. Solid-State Lett.* **2004**, *7*, A442.
[26] B. Li, M. Xu, T. Li, W. Li, S. Hu, *Electrochem. Commun.* **2012**, *17*, 92.
[27] G. H. Wrodnigg, J. O. Besenhard, M. Winter, *J. Electrochem. Soc.* **1999**, *146*, 470.
[28] P. Verma, P. Novák, *Carbon* **2012**, *50*, 2599.
[29] L. J. Fu, J. Gao, T. Zhang, Q. Cao, L. C. Yang, Y. P. Wu, R. Holze, *J. Power Sources* **2007**, *171*, 904.
[30] M. Nie, D. P. Abraham, D. M. Seo, Y. Chen, A. Bose, B. L. Lucht, *J. Phys. Chem. C* **2013**, *117*, 25381.
[31] S. K. Jeong, M. Inaba, Y. Iriyama, T. Abe, Z. Ogumi, *J. Power Sources* **2008**, *175*, 540.
[32] P. G. Kitz, M. J. Lacey, P. Novák, E. J. Berg, *Anal. Chem.* **2019**, *91*, 2296.